

# Plasmonic generation of ultrashort extreme-ultraviolet light pulses

In-Yong Park<sup>1†</sup>, Seungchul Kim<sup>1†</sup>, Joonhee Choi<sup>1†</sup>, Dong-Hyub Lee<sup>1</sup>, Young-Jin Kim<sup>1</sup>, Matthias F. Kling<sup>2</sup>, Mark I. Stockman<sup>3</sup> and Seung-Woo Kim<sup>1\*</sup>

**Ultrashort extreme-ultraviolet pulses are a key tool in time-resolved spectroscopy for the investigation of electronic motion in atoms<sup>1,2</sup>, molecules<sup>3</sup> and solids<sup>4</sup>. High-harmonic generation is a well-established process for producing ultrashort extreme-ultraviolet pulses by direct frequency upconversion of femtosecond near-infrared pulses<sup>5–7</sup>. However, elaborate pump-probe experiments performed on the attosecond time-scale<sup>8,9</sup> require continuous efforts to improve the spatiotemporal coherence and also the repetition rate of the generated pulses. Here, we demonstrate a three-dimensional metallic waveguide for the plasmonic generation of ultrashort extreme-ultraviolet pulses by means of field enhancement using surface-plasmon polaritons. The intensity enhancement factor reaches a peak of  $\sim 350$ , allowing generation up to the 43rd harmonic in xenon gas, with a modest incident intensity of  $\sim 1 \times 10^{11} \text{ W cm}^{-2}$ . The pulse repetition rate is maintained as high as 75 MHz without external cavities. The plasmonic waveguide is fabricated on a cantilever microstructure and is therefore suitable for near-field spectroscopy with nanometre-scale lateral selectivity.**

Surface-plasmon polaritons (SPPs) are described as the electromagnetic wave propagating along a metal–dielectric interface that results from coupling between incident photons and surface plasmons<sup>10,11</sup>. In nanostructured tapered waveguides, SPPs can be controlled to adiabatically follow the geometric shape of the waveguide and asymptotically stop at the tip of the taper where the local cross-sectional dimension becomes infinitesimally small<sup>12,13</sup>. As a result, SPPs can be focused beyond the diffraction limit in three dimensions on a sub-wavelength spot, with drastically enhanced optical intensity<sup>12–14</sup>. The effect of SPP adiabatic nanofocusing has been confirmed, studied and also tested for nanometre-scale microscopy in a series of earlier experiments<sup>15–19</sup>.

In our investigation, this intriguing phenomenon of SPP adiabatic nanofocusing is used to generate ultrashort extreme ultraviolet (EUV) pulses directly from near-infrared (NIR) pulses. As depicted in Fig. 1, a three-dimensional waveguide was devised to concentrate the incident NIR pulses into a sub-wavelength spot, allowing high-harmonic generation of EUV light pulses to take place with high spatiotemporal coherence. The waveguide is a metallic nanostructure made of silver and has a hollow hole that takes the shape of a tapered cone with its elliptical cross-section decreasing from the inlet aperture (minor-axis diameter,  $\sim 2 \mu\text{m}$ ) to the exit aperture (minor-axis diameter,  $\sim 100 \text{ nm}$ ). The incident NIR pulses are focused on the inlet aperture at a repetition rate of 75 MHz with a moderate intensity of  $\sim 1 \times 10^{11} \text{ W cm}^{-2}$ . While each NIR pulse propagates through the tapered hole towards the exit aperture, the electric field intensity inside the hole undergoes a substantial

boost that is sustained by the SPPs driven by the incident NIR pulse. Consequently, high-harmonic EUV pulses are generated exactly where the enhanced field reaches its peak near the exit aperture. Gaseous atoms are supplied into the waveguide by controlling the pressure difference between the inlet and exit apertures. The peak intensity enhancement factor exceeds 20 dB, requiring no additional pulse amplification to reach the threshold intensity necessary to trigger the ionization process leading to high-harmonic generation. The pulse repetition rate of the incident NIR pulses is maintained during the generation process.

The tapered waveguide used in our experiment is geometrically characterized by four parameters, as shown in Fig. 2c: the elliptic ratio of the cross-section ( $r = b/a$ ), the minor-axis diameter of the exit aperture ( $d$ ), the cone angle defined in the minor-axis plane ( $\theta$ ) and cone height ( $h$ ). A finite-difference time-domain (FDTD) simulation was conducted to determine the values of the four geometrical parameters necessary to yield an optimum pattern of field enhancement for high-harmonic generation within the waveguide (see Methods for simulation conditions). By a series of trial-and-error computations, these parameters were determined to be  $r = 0.5$ ,  $d = 100 \text{ nm}$ ,  $\theta = 14^\circ$  and  $h = 9 \mu\text{m}$ . Figure 2a shows the intensity field computed within the designed waveguide. The intensity enhancement factor exceeded 20 dB with a peak of  $\sim 350$  over a near-cylindrical volume (diameter,  $\sim 240 \text{ nm}$ ; length,  $\sim 450 \text{ nm}$ ) near the exit aperture. Compared with bowties<sup>20</sup> or nanorods<sup>21</sup>, which have previously been used for field enhancement through stationary resonance of localized surface plasmons, the net volume of 20 dB intensity enhancement turns out to be three orders of magnitude larger than that of a single bowtie element or nanorod. This improvement is attributed to the strong concentration of the converging SPPs that gradually accumulate towards the exit aperture along the three-dimensional tapered waveguide.

Figure 2b presents three consecutive snapshots that show how the field intensity builds up strongly near the exit aperture. The incident NIR pulse turns into a plasmonic wave as it progressively couples with the SPPs produced in the waveguide. The plasmonic wave maintains the fundamental anti-symmetric mode of propagation inside the waveguide, and cannot therefore escape through the small exit aperture. Consequently, the plasmonic wave reverses its propagation direction at the point where the minor-axis diameter of the tapered waveguide reduces to below half its wavelength<sup>22–24</sup>. This cutoff effect gives rise to a counter-propagating wave that subsequently interferes with the incoming wave. As a result, the combined wave forms a standing field near the exit aperture, which gives a fourfold increase in peak intensity compared to the incoming wave alone. Our simulation also confirms that an elliptic

<sup>1</sup>Ultrafast Optics for Ultraprecision Group, Korea Advanced Institute of Science and Technology (KAIST), Daejeon, 305-701, South Korea, <sup>2</sup>Max Planck Institute of Quantum Optics, Hans-Kopfermann-Str. 1, D-85748 Garching, Germany, <sup>3</sup>Department of Physics and Astronomy, Georgia State University, Atlanta, Georgia 30303, USA; <sup>†</sup>These authors contributed equally to this work as main authors. \*e-mail: swk@kaist.ac.kr

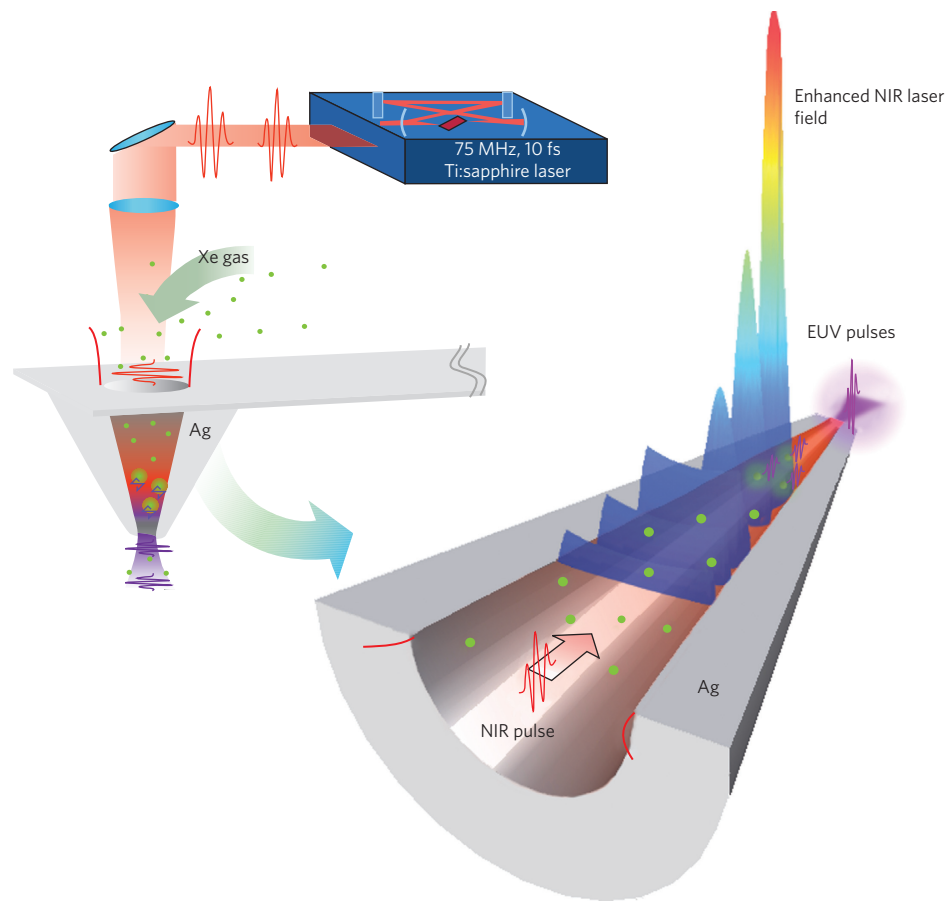


**Figure 1 | Plasmonic nanofocusing of femtosecond NIR light pulses for high-harmonic generation of coherent ultrashort EUV pulses using a metallic waveguide.** Surface-plasmon polaritons are guided to converge to a sub-wavelength spot near the exit aperture, creating a strong boost in the intensity field of incident NIR pulses propagating along the waveguide. EUV pulses produced by means of high-harmonic generation through interaction with xenon gaseous atoms emanate through the exit aperture, while the driving NIR pulses are predominantly reflected backwards.

cross-section ( $r = 0.5$ ) is more beneficial than a circular one with  $r = 1.0$ , which achieves a maximum intensity enhancement of only  $\sim 180$ . Furthermore, the enhanced plasmonic field suffers no significant group delay dispersion (only  $\sim 15 \text{ fs}^2$ ), with a tiny plasmonic ring-down oscillation at the pulse tail.

For proof-of-concept experiments, the waveguide was fabricated on a cantilever microstructure using a focused-ion beam (FIB) milling process (see Fig. 3 and Methods for a detailed explanation of fabrication). A series of experiments was then performed to validate the effectiveness of the fabricated waveguide in generating EUV radiation (see Fig. 4 and Methods for experimental conditions). The high-harmonic spectrum of the generated EUV radiation was first observed by using a transmission diffraction grating (Fig. 4a,b). The measured spectrum successfully demonstrated the high harmonics in the generated EUV radiation (Fig. 4c): H15 to H27 harmonics in the plateau and H29 to H43 in the cutoff region. The nanometre-sized source implies a high spatial dispersion of the generated EUV light, which affects the spectral resolution in the spectra obtained with our set-up. We estimate the resolution in the range of H15 to H43 to be 0.5–5.5 eV.

The observed high harmonics were cross-checked by measuring the divergence angles formed when they were emitted from the exit aperture. For this purpose, four different metal filters were prepared (Fig. 4d): a 200-nm-thick aluminium filter, a 200-nm-thick germanium filter combined with a 200-nm-thick aluminium sheet, a 100-nm-thick Parylene filter bonded on both sides with a 25 nm sheet of aluminium, and a 500-nm-thick zirconium filter. Their transmission spectral ranges were 20–80 nm, 40–60 nm, 1–40 nm

and 1–20 nm, respectively<sup>25</sup>. With the diffraction grating removed, the transverse intensity distribution of the EUV radiation was then monitored by moving the photomultiplier tube along the major axis, yielding different divergence angles for the filters (Fig. 4d):  $32^\circ$  for the aluminium filter,  $20^\circ$  for the germanium filter,  $13^\circ$  for the Parylene filter and  $6^\circ$  for the zirconium filter (Fig. 4d). Substituting the measured divergence angles into Fraunhofer diffraction theory<sup>26</sup> confirmed the longest wavelength transmitted by each filter, together with its corresponding high-harmonic order: 73 nm (H11) for the aluminium filter, 53 nm (H15) for the germanium filter, 38 nm (H21) for the Parylene filter and 18.6 nm (H43) for the zirconium filter.

No phase-matching was required when observing any of the harmonics, because their generation was naturally confined only to the sub-wavelength spot with a length of  $\sim 400 \text{ nm}$  where the enhanced plasmonic field exceeded the intensity threshold of ionization. The conversion efficiency was estimated by counting the photon numbers while moving the photomultiplier tube across the entire diffraction area for each filter. The photon number measured for H15 and H17 harmonics was  $\sim 1 \times 10^9$  photons/s, corresponding to a conversion efficiency of  $\sim 1 \times 10^{-8}$ . This result is about 100 times higher than that measured for a 150-bowtie antenna array<sup>27</sup>. The photon flux for each higher harmonic in the cutoff region was on the scale of  $\sim 1 \times 10^7$  photons/s. It is also worth noting that the exit aperture is small enough to block not only the incident NIR pulses, but also lower harmonics below 5th order. Neither thermal damage nor optical breakdown was observed throughout our experiment, because the silver-coated cantilever structure

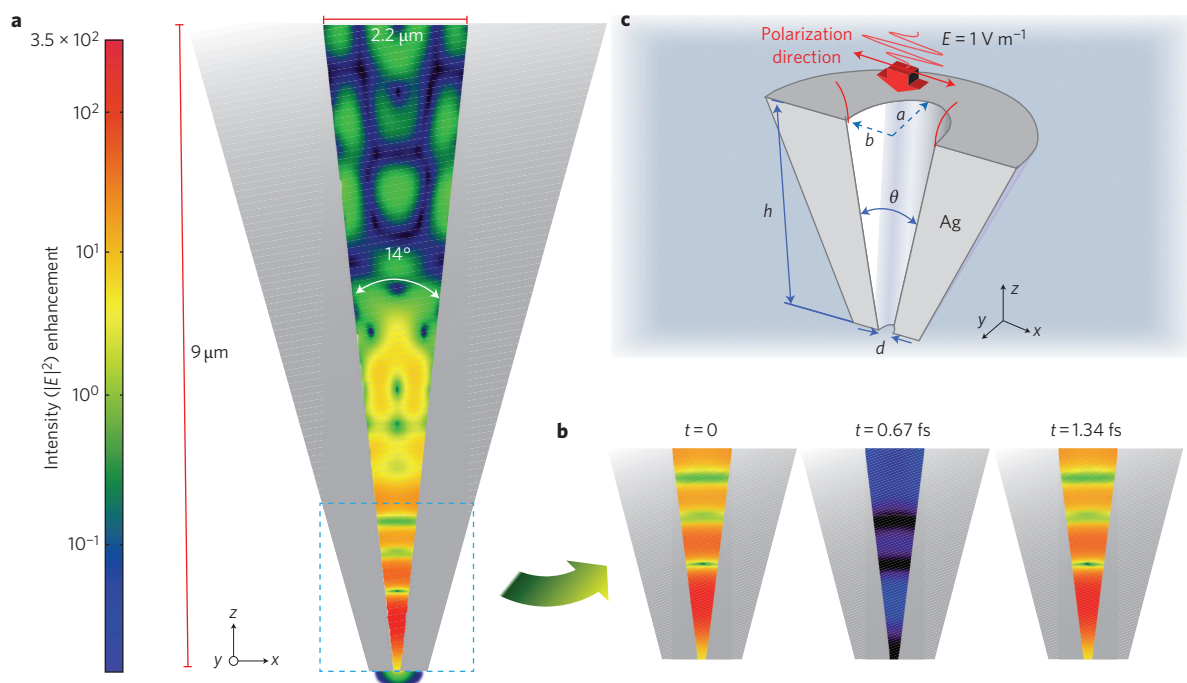


**Figure 2 | Computation of the enhanced electric field inside the waveguide by adopting a FDTD method.** **a**, Snapshot illustrating the intensity distribution at the moment when the intensity peak of the incident NIR pulse approaches the exit aperture. **b**, Three consecutive snapshots in time steps of 0.67 fs, confirming the interferometric creation of a standing-wave field by the counter-propagating plasmonic field upon reflection from the exit aperture. **c**, Four geometrical parameters considered in designing the waveguide (where  $r = b/a$ ).

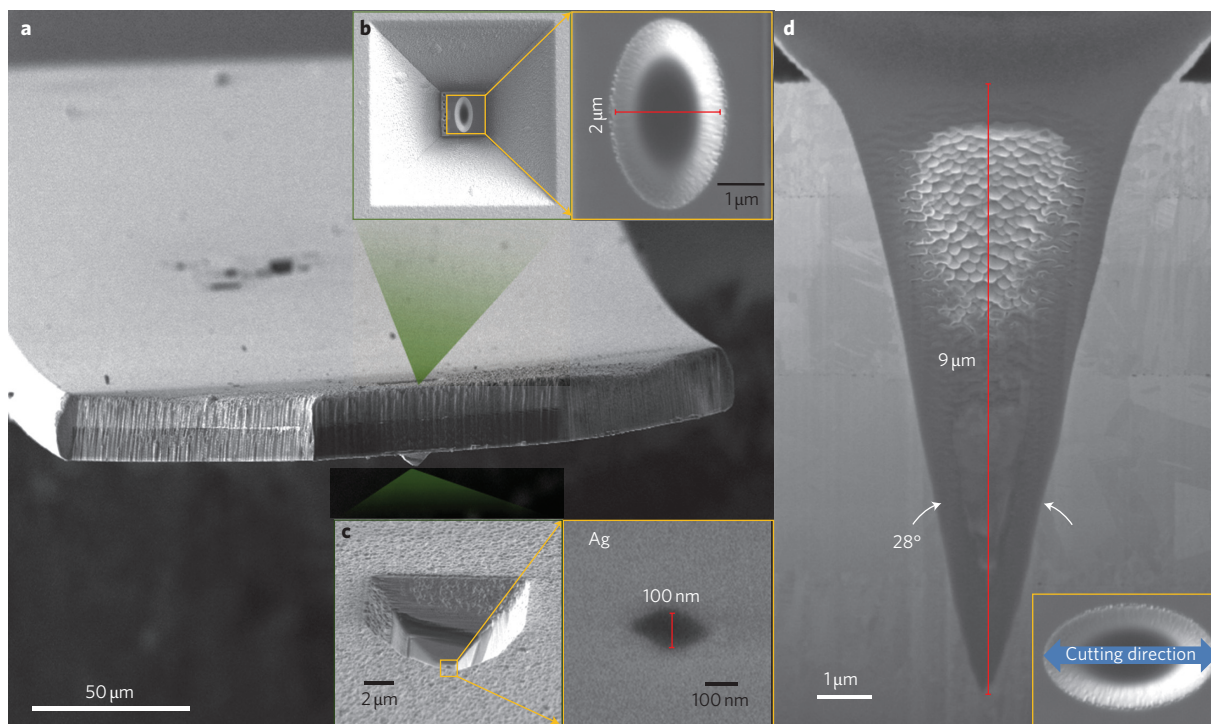


**Figure 3 | Waveguide fabrication on the tip of a cantilever microstructure using the FIB process.** **a**, Scanning electron microscope (SEM) image of the cantilever structure that houses the waveguide. **b**, Top view showing the inlet aperture of the waveguide. **c**, Bottom view showing the exit aperture. **d**, Cross-sectional view cut along the major axis of the elliptical profile of the waveguide.

holding the waveguide absorbed heat well and also functioned as a good conductor.

In conclusion, the tapered waveguide of the present elliptical hollow cross-section proved to be an effective means with

which to carry out plasmonic nanofocusing of NIR pulses for high-harmonic generation of ultrashort EUV pulses with high spatiotemporal coherence. The intensity enhancement factor exceeds 20 dB, directly generating high harmonics up to 43rd

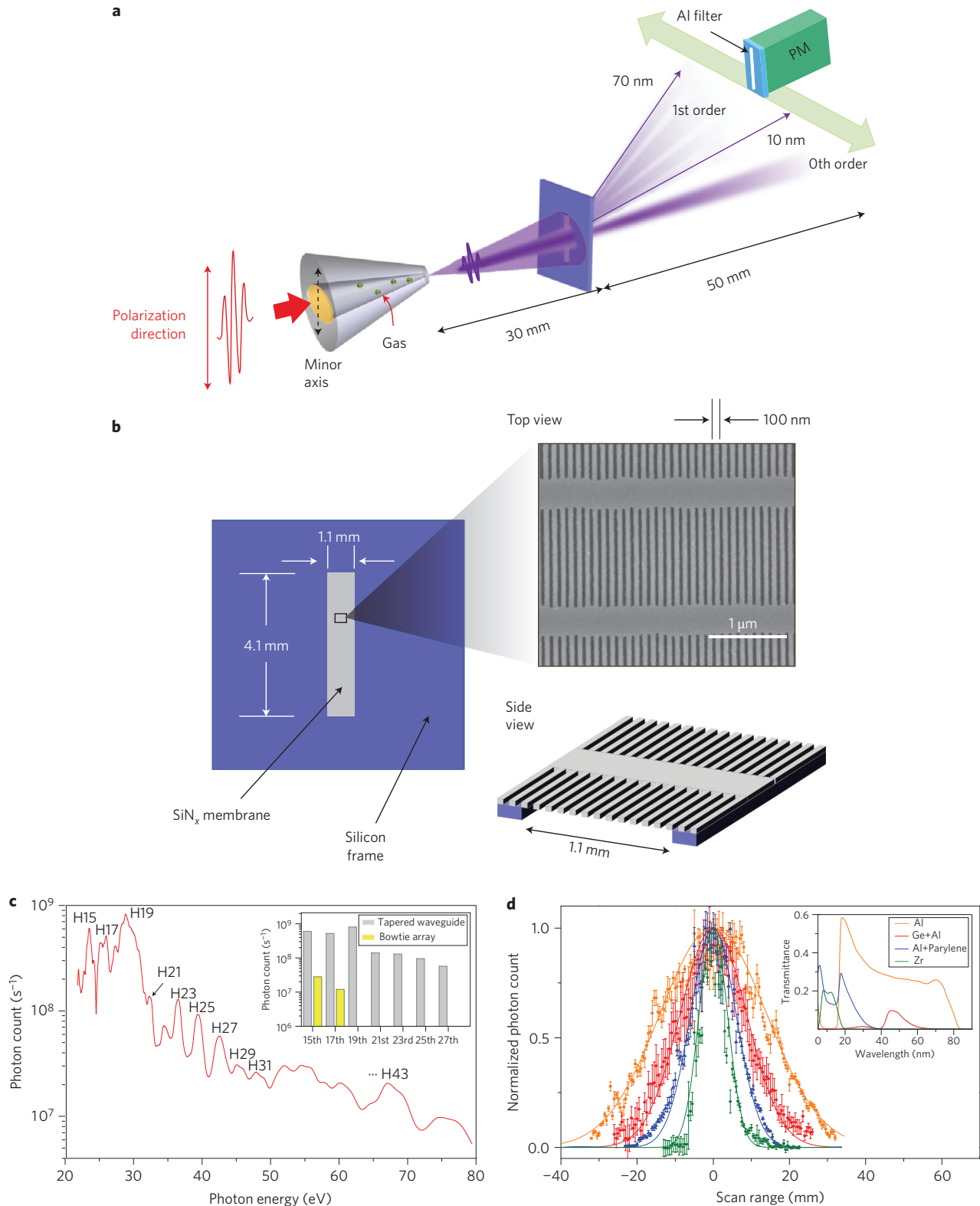


**Figure 4 | Experimental results.** **a**, Measurement scheme using a transmission-type diffraction grating and a photomultiplier (PM) tube. **b**, SEM images of the grating showing the important dimensions. **c**, Measured spectrum spanning from the 15th (H15) to 43rd (H43) harmonics. Inset: comparison of photon counts with the bowtie array of ref. 27. **d**, Transverse intensity distributions measured with different band-pass spectral filters (inset). Curves were obtained with the grating removed while the PM tube was moved in steps of 0.5 mm. The PM tube was located at a distance of 60 mm from the tip. Error bars indicate standard deviation of 10 repeated samplings taken at a given location.

order from a modest input intensity of  $1 \times 10^{11} \text{ W cm}^{-2}$  in an interaction with xenon gaseous atoms. In comparison to previous studies using planar nanostructures<sup>27</sup> with bowtie or nanorod

shapes, this three-dimensional waveguide, as well as offering high conversion efficiency, also provides improved immunity to thermal damage and optical breakdown. The waveguide structure

can be readily embedded on a cantilever tip to render it suitable for a range of near-field experiments in attosecond science, including time-resolved pump-probe spectroscopy and photoelectron emission microscopy.

## Methods

**FDTD simulation.** The waveguide structure was modelled using hexahedron grids (5 nm × 5 nm × 5 nm) in three dimensions. The incident NIR pulses were assumed to have a temporal duration of 10 fs with a 100 nm spectral width centred at a wavelength of 800 nm. The wavelength-dependent dielectric constant of the waveguide material (silver) was estimated by means of a modified Debye model<sup>28</sup>. The polarization direction of the incident pulses was set parallel to the minor axis of the elliptical cross-section of the inlet aperture.

**Waveguide fabrication.** The three-dimensional waveguide designed by FDTD simulation was fabricated on a commercially available cantilever microstructure for near-field optical microscopy (Nascatec GmbH). The cantilever was delivered with a built-in hollow pyramid-shaped tip made of silicon nitride. In the first step of the fabrication process, the hollow tip was filled from the bottom with platinum (to a thickness of 3.5 μm), and a 10 μm layer of silver was then deposited on top of the platinum layer. The designed elliptical profile was carved in the silver layer by FIB milling. Specifically, the entire three-dimensional elliptical inner void volume of the waveguide was divided into a total of 31 horizontally flat laminates that were etched, one by one, to a depth of ~300 nm from the inlet surface towards the exit aperture. The bottom surface of the tip was finally polished flat from the outside until the exit aperture had a diameter of 100 nm in the minor-axis direction.

**Experimental set-up.** The fabricated waveguide was placed in a vacuum chamber where the operating pressure was kept below  $1 \times 10^{-4}$  torr. The NIR pulses used in the experiment were delivered from a Ti:sapphire oscillator (Femtolasers, Femtosource sPro) at a repetition rate of 75 MHz. Each pulse had an average power of 1 nJ with a duration of 10 fs. The spectral width was 100 nm, centred at a wavelength of 800 nm. The NIR pulses were focused via an aspheric lens to a 5-μm-diameter spot on the inlet aperture, which had elliptical major- and minor-axis diameters of 4.4 μm and 2.2 μm, respectively. The focused spot yielded an intensity of  $5 \times 10^{11}$  W cm<sup>-2</sup>, which was two orders of magnitude lower than the threshold intensity required for high-harmonic generation. The entire sub-assembly of the waveguide was contained in a gas cell with dimensions of 11 mm × 11 mm × 3 mm, inside which xenon gaseous atoms were supplied with a controlled pressure of 70 torr. The gas cell was fitted with a 150-μm-thick Al<sub>2</sub>O<sub>3</sub> window to allow the NIR pulses to enter, as well as a through-hole with a diameter of 1 mm to enable the generated EUV radiation to escape without reflection losses.

**Spectral characterization.** The diffraction grating (nm<sup>2</sup> LLC, custom-made) comprised a free-standing line array of bars with a pitch of 100 nm, fabricated on a 160-nm-thick membrane of silicon nitride using a through-etching process<sup>29,30</sup>. The effective area was 1.1 mm × 4.1 mm (Fig. 4b) with a diffraction efficiency of ~20%. The first-order diffracted beam of the incident EUV radiation was aligned to spread over an angle of 6–44° from the grating surface normal to allow wavelengths of 10–70 nm to be monitored with a photomultiplier tube (Photonis, Model 4751). The photomultiplier tube was sensitive only to short wavelengths below 100 nm and was covered with an aluminium filter to prevent it from being disturbed by leaked NIR fundamental or stray lower harmonics.

Received 21 August 2011; accepted 7 September 2011;  
published online 16 October 2011

## References

1. Uiberacker, M. *et al.* Attosecond real-time observation of electron tunnelling in atoms. *Nature* **446**, 627–632 (2007).
2. Schultze, M. *et al.* Delay in photoemission. *Science* **328**, 1658–1662 (2010).
3. Sansone, G. *et al.* Electron localization following attosecond molecular photoionization. *Nature* **465**, 763–766 (2010).
4. Cavalieri, A. L. *et al.* Attosecond spectroscopy in condensed matter. *Nature* **449**, 1029–1032 (2007).
5. Krausz, F. & Ivanov, M. Attosecond physics. *Rev. Mod. Phys.* **81**, 163–234 (2009).
6. Popmintchev, T., Chen, M.-C., Arpin, P., Murnane, M. M. & Kapteyn, H. C. The attosecond nonlinear optics of bright coherent X-ray generation. *Nature Photon.* **4**, 822–832 (2010).
7. Jones, R. J., Moll, K. D., Thorpe, M. J. & Ye, J. Phase-coherent frequency combs in the vacuum ultraviolet via high-harmonic generation inside a femtosecond enhancement cavity. *Phys. Rev. Lett.* **94**, 193201 (2005).

8. Krütschek, R. *et al.* Ultraviolet enhancement cavity for ultrafast nonlinear optics and high-rate multiphoton entanglement experiments. *Nature Photon.* **4**, 170–173 (2010).
9. Gohle, C. *et al.* A frequency comb in the extreme ultraviolet. *Nature* **436**, 234–237 (2005).
10. Gramotnev, D. K. & Bozhevolnyi, S. I. Plasmonics beyond the diffraction limit. *Nature Photon.* **4**, 83–91 (2010).
11. Stockman, M. I. Nanoplasmonics: the physics behind the applications. *Phys. Today* **64**, 39–44 (2011).
12. Stockman, M. I. Nanofocusing of optical energy in tapered plasmonic waveguides. *Phys. Rev. Lett.* **93**, 137404 (2004).
13. Babajanyan, A. J., Margaryan, N. L. & Nerkararyan, K. V. Superfocusing of surface polaritons in the conical structure. *J. Appl. Phys.* **87**, 3785–3788 (2000).
14. Gramotnev, D. K., Vogel, M. W. & Stockman, M. I. Optimized nonadiabatic nanofocusing of plasmons by tapered metal rods. *J. Appl. Phys.* **104**, 034311 (2008).
15. Verhagen, E., Polman, A. & Kuipers, L. Nanofocusing in laterally tapered plasmonic waveguides. *Opt. Express* **16**, 45–57 (2008).
16. Verhagen, E., Spasenovic, M., Polman, A. & Kuipers, L. Nanowire plasmon excitation by adiabatic mode transformation. *Phys. Rev. Lett.* **102**, 203904 (2009).
17. De Angelis, F. *et al.* A hybrid plasmonic-photonic nanodevice for label-free detection of a few molecules. *Nano Lett.* **8**, 2321–2327 (2008).
18. De Angelis, F. *et al.* Nanoscale chemical mapping using three-dimensional adiabatic compression of surface plasmon polaritons. *Nature Nanotech.* **5**, 67–72 (2010).
19. Ropers, C. *et al.* Grating-coupling of surface plasmons onto metallic tips: a nano-confined light source. *Nano Lett.* **7**, 2784–2788 (2007).
20. Kinkhabwala, A. *et al.* Large single-molecule fluorescence enhancements produced by a bowtie nanoantenna. *Nature Photon.* **3**, 654–657 (2009).
21. Mühlischlegel, P., Eisler, H.-J., Martin, O. J. F., Hecht, B. & Pohl, D. W. Resonant optical antennas. *Science* **308**, 1607–1609 (2005).
22. Choi, H., Pile, D. F., Nam, S., Bartal, G. & Zhang, X. Compressing surface plasmons for nano-scale optical focusing. *Opt. Express* **17**, 7519–7524 (2009).
23. Novotny, L. & Hafner, C. Light propagation in a cylindrical waveguide with a complex, metallic, dielectric function. *Phys. Rev. E* **50**, 4094–4106 (1994).
24. Ginzburg, P., Arbel, D. & Orenstein, M. Gap plasmon polariton structure for very efficient microscale-to-nanoscale interfacing. *Opt. Lett.* **31**, 3288–3290 (2006).
25. Henke, B. L., Gullikson, E. M. & Davis, J. C. X-ray interactions: photoabsorption, scattering, transmission, and reflection at  $E = 50$ –30,000 eV,  $Z = 1$ –92. *At. Data. Nucl. Data. Tables* **54**, 181–342 (1993).
26. Kathuria, Y. P. Fresnel and far-field diffraction due to an elliptical aperture. *J. Opt. Soc. Am. A* **2**, 852–857 (1985).
27. Kim, S. *et al.* High harmonic generation by resonant plasmon field enhancement. *Nature* **453**, 757–760 (2008).
28. Gai, H., Wang, J. & Tian, Q. Modified Debye model parameters of metals applicable for broadband calculations. *Appl. Opt.* **46**, 2229–2233 (2007).
29. Vamvakas, V. Em., Vourdas, N. & Gardelis, S. Optical characterization of Si-rich silicon nitride films prepared by low pressure chemical vapour deposition. *Microelectron. Reliab.* **47**, 794–797 (2007).
30. Kornilov, O., Wilcox, R. & Gessner, O. Nanograting-based compact vacuum ultraviolet spectrometer and beam profiler for *in situ* characterization of high-order harmonic generation light sources. *Rev. Sci. Instrum.* **81**, 063109 (2010).

## Acknowledgements

This work was supported by the Creative Research Initiative Program, the National Space Laboratory Program and the Basic Science Research Program (2010-0024882) funded by the National Research Foundation of the Republic of Korea. M.F.K. acknowledges support by the German Science Foundation through the Emmy-Noether programme and SPP1391 and by the BMBF through the PhoNa network. The work of M.I.S. was supported by the Chemical Sciences, Biosciences and Geosciences Division (grant no. DEFG02-01ER15213) and the Materials Sciences and Engineering Division (grant no. DE-FG02-11ER46789) of the Office of Basic Energy Sciences, Office of Science, US Department of Energy.

## Author contributions

The project was planned by S.-W.K., S.K., I.-Y.P. and J.C. The simulation and experiment were performed by I.-Y.P., S.K., J.C. and D.-H.L. Spectral characterization of the higher harmonics was contributed by M.F.K. All authors discussed the results and contributed to the final manuscript.

## Additional information

The authors declare no competing financial interests. Reprints and permission information is available online at <http://www.nature.com/reprints>. Correspondence and requests for materials should be addressed to S.-W.K.